AN INVESTIGATION ON THE FLOW THROUGH A HYPERSONIC NOZZLE IN SHOCK-GUN TUNNEL

SHIGEO UCHIDA, KOSEI KUWABARA,
and KUNIYOSHI FURUHASHI

Department of Aeronautical Engineering

(Received October 30, 1970)

1. Introduction

A preliminary investigation on the compressible flow through a conical nozzle is reported. Connecting with the analytic solution of transonic flow at the throat area, super- to hypersonic flow is calculated by the method of characteristics, which is shown in a convenient form for the numerical calculations. Experiments on the flow through a hypersonic nozzle of $M=10$ are also performed in the shock-gun tunnel. It is found that the results agree fairly well with analytical calculations.

2. Shock-Gun Tunnel

The main facility of shock-gun tunnel in Nagoya University consists of six main parts, *i.e.* driver tube No. 1 and No. 2, driven tube No. 1 and No. 2, nozzle section and dump tank, which are connected by three motor-driven connecting nuts as shown in Fig. 1. This construction enables us multi-purpose use of the

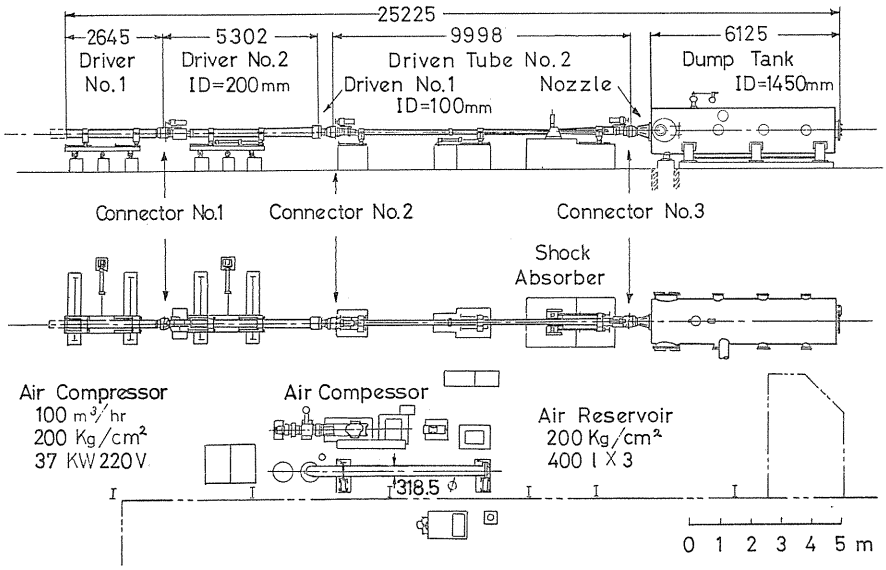

FIG. 1. General view of the shock-gun tunnel.

following four ways.

(*i*) *Shock tunnel:* Two stage metal plates are put in the connector No. 2. Flows in the shock tunnel can be started by evacuating the gas in intermediate section of these two plates.

(*ii*) *Gun tunnel:* A nylon piston of 0.220 to 0.500 kg is inserted in the end of driven tube No. 2, and the same proccess is used to start the flows.

(*iii*) *Shock-gun tunnel of heavy piston type:* A heavy piston of 8.255 kg is inserted in the upper end of driver tube No. 2. The metal plate in the connector

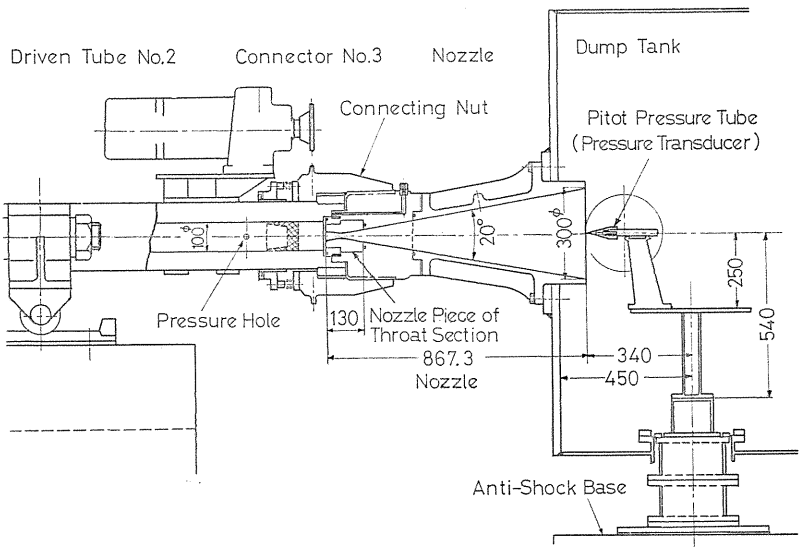

FIG. 2. General arrangement of the nozzle section.

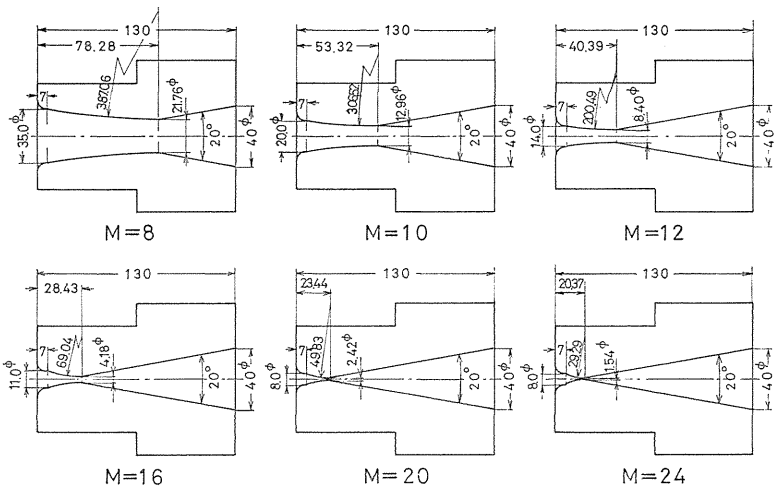

FIG. 3. The nozzle pieces of throat section.

No. 1 is broken by the high pressure of air charged in the driver tube No. 1. The heavy piston makes a high energy gas at the downstream end of driver tube No. 2, which enables to drive the shock-gun tunnel in a higher energy level.

(*iv*) *High speed range:* A piston in driven tube No. 2 is designated to carry a flight model, which makes a free flight in the dump tank.

The hypersonic nozzle at the downstream end of driven tube No. 2 consists of two parts, *i.e.* the main part of the conical nozzle of angle 20° and the nozzle piece of throat section, which can be easily changed to make flows of $M=8$, 10, 12, 16, 20 and 24. The general arrangement of nozzle section, which is connected with the driven tube No. 2 by the connector No. 3, is shown in Fig. 2. The connecting nut is chain-driven by the electric motor and is screwed into the nozzle section. The detail of the nozzle piece of throat section for $M=10$ is shown in Fig 3.

3. Analysis of Hypersonic Flow Through a Conical Nozzle

(*a*) *Transonic flow through the throat area of a convergent-divergent nozzle*

Several methods[1] have been developed for the analysis of transonic flow through the throat area of a convergent-divergent nozzle shown in Fig. 4. In this preliminary investigation calculations are performed by the use of Oswatitsch and Rothstein's method[2], which will be briefly described in the followings.

The velocity components, u and v, are assumed to form the following power series expansion as the first order approximation.

$$u = A_0 + A_1 y + A_2 y^2, \quad v = B_0 + B_1 y \qquad (1)$$

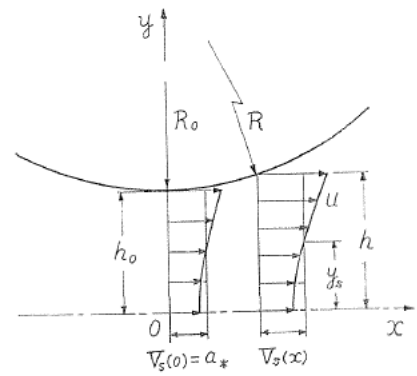

FIG. 4. Transonic flow through the throat area.

Boundary conditions are

$$v = 0 \text{ at } y = 0; \quad v = V_s h' \text{ at } y = h \qquad (2)$$

where V_s is the sectional mean velocity calculated by the one-dimensional flow theory. Substituting Eq. (1) into Eq. (2), B_0 and B_1 should be

$$B_0 = 0 \text{ and } B_1 = V_s(h'/h) \qquad (3)$$

The condition of irrotationality

$$v_x - u_y = 0 \qquad (4)$$

is satisfied, when

$$A_1 = B_0' = 0 \text{ and } A_2 = B_1'/2 = (1/2)(V_s h'/h)'. \qquad (5)$$

Introducing y_s, which is the y coordinate to give $u = V_s$, we have

$$u = V_s + A_2(y^2 - y_s^2). \tag{6}$$

This means that A_0 can be substituted by $A_0 = V_s - A_2 y_s^2$.

In transonic approximations the mass flow density near the throat section is calculated by

$$\begin{aligned}\rho V \fallingdotseq \rho u &= \rho_* a_* \Big[1 - \frac{\gamma+1}{2}\Big\{\Big(\frac{V_s}{a_*} - 1\Big) + \Big(\frac{u}{a_*} - \frac{V_s}{a_*}\Big)\Big\}^2 + \cdots\Big] \\ &\fallingdotseq \rho_* a_* \Big[\frac{\rho_s V_s}{\rho_* a_*} - (\gamma+1)\Big(\frac{V_s}{a_*} - 1\Big)\frac{A_2}{a_*}(y^2 - y_s^2) - \frac{\gamma+1}{2}\Big(\frac{A_2}{a_*}\Big)^2 (y^2 - y_s^2)^2 + \cdots\Big].\end{aligned} \tag{7}$$

The mass flow through nozzle is given by

$$\begin{aligned}G = \int_0^h \rho u \cdot 2\pi y dy &= \pi \rho_* a_* h^2 \Big[\frac{\rho_s V_s}{\rho_* a_*} \\ &- 2(\gamma+1)\Big(\frac{V_s}{a_*} - 1\Big)\frac{A_2}{a_*}\Big(\frac{h^2}{4} - \frac{y_s^2}{2}\Big) - (\gamma+1)\Big(\frac{A_2}{a_*}\Big)^2\Big(\frac{h^4}{6} - \frac{h^2 y_s^2}{2} + \frac{y_s^4}{2}\Big) + \cdots\Big].\end{aligned} \tag{8}$$

In the choking condition G attains its maximum value. Calculating the condition $dG/dy_s = 0$ at the throat section, where $V_s/a_* = 1$, we have

$$y_s^2 = h^2/2. \tag{9}$$

For the first order approximation Eq. (9) holds in the neighbourhood of throat section. Using this value the maximum of G is obtained by

$$\begin{aligned}G_{\max} &= \pi \rho_* a_* h_0^2 [1 - (1/96)(\gamma+1)(hh'')_{x=0}^2] \\ &= \pi \rho_* a_* h_0^2 [1 - (1/96)(\gamma+1)(h_0/R_0)^2]\end{aligned} \tag{10}$$

where $R \fallingdotseq h''(x)$ is the radius of curvature of wall at the throat section.

In the transonic region of throat area h' becomes a higher order small quantity, and, therefore,

$$A_2 = (1/2)(V_s h'/h)' \fallingdotseq (V_s/2)(h_0''/h_0). \tag{11}$$

Velocity components can be obtained with this value of A_2 as follows:

$$\begin{aligned}\frac{u}{a_*} &= \frac{V_s}{a_*}\Big[1 + \frac{1}{2}h_0'' h_0\Big(\frac{y^2}{h^2} - \frac{1}{2}\Big)\Big] = \frac{V_s}{a_*}\Big[1 + \frac{1}{2}\frac{h_0}{R_0}\Big(\frac{y^2}{h^2} - \frac{1}{2}\Big)\Big] \\ \frac{v}{a_*} &= \frac{V_s}{a_*}\frac{h'}{h}y = \frac{V_s}{a_*}h'\Big(\frac{y}{h}\Big)\end{aligned} \tag{12}$$

where v/a_* is negligible comparing with u/a_*. From the one-dimensional flow theory, we have

$$\begin{aligned}\frac{V_s}{a_*} &= 1 + \sqrt{\frac{2}{\gamma+1}}\Big(\frac{h_0''}{h_0}\Big)^{1/2} x + \Big[-\frac{2\gamma-3}{3(\gamma+1)}\frac{h_0''}{h_0} + \frac{1}{6}\sqrt{\frac{2}{\gamma+1}}\frac{h_0'''/h_0}{(h_0''/h_0)^{1/2}}\Big]x^2 + \cdots \\ &= 1 + \sqrt{\frac{2}{\gamma+1}}\Big(\frac{h_0}{R_0}\Big)^{1/2}\frac{x}{h_0} + \cdots.\end{aligned} \tag{13}$$

Neglecting the second order terms, flow speed is given by substituting Eq. (13)

into Eq. (12).

$$\frac{V}{a_*} \fallingdotseq \frac{u}{a_*} = 1 + \sqrt{\frac{2}{\gamma+1}}\left(\frac{h_0}{R_0}\right)^{1/2}\frac{x}{h_0} + \frac{1}{2}\frac{h_0}{R_0}\left(\frac{y^2}{h_0^2} - \frac{1}{2}\right) + \cdots. \tag{14}$$

Curves of V/a_*=constant give the constant speed lines.

(*b*) *Theory of characteristics for an axisymmetric flow*

The supersonic flow in a nozzle can be solved by the method of characteristics, where singularities along the axis should be taken account for the flow of axial symmetry.

Taking x, y coordinates in the meridian plane, an axisymmetric compressible flow of non-viscous fluid is governed by the gas dynamics equation and condition of irrotationality, respectively, given

$$\left(1 - \frac{u^2}{a^2}\right)\frac{\partial u}{\partial x} - \frac{uv}{a^2}\frac{\partial u}{\partial y} - \frac{uv}{a^2}\frac{\partial v}{\partial x} + \left(1 - \frac{v^2}{a^2}\right)\frac{\partial v}{\partial y} + \varepsilon\frac{v}{y} = 0 \tag{15}$$

$$-\frac{\partial u}{\partial y} + \frac{\partial v}{\partial x} = 0 \tag{16}$$

$$a^2 = a_\infty^2 - \{(\gamma-1)/2\}(u^2 + v^2 - U_\infty^2) \tag{17}$$

where, u, v are x, y components of velocity vector, respectively, and ε convention is taken 1 for axisymmetric flow and 0 for two-dimensional flow.

For the general expression of a system of quasi-linear partial differential equation

$$\begin{aligned} A_1u_x + B_1u_y + C_1v_x + D_1v_y + E_1 = 0 \\ A_2u_x + B_2u_y + C_2v_x + D_2v_y + E_2 = 0 \end{aligned} \tag{18}$$

ξ- and η branches of characteristics are given by

$$\begin{aligned} &y_\xi - \lambda_+ x_\xi = 0\,; \quad Tu_\xi + (a\lambda_+ - S)v_\xi + (L\lambda_+ - M)x_\xi = 0 \\ &y_\eta - \lambda_- x_\eta = 0\,; \quad Tu_\eta + (a\lambda_- - S)v_\eta + (L\lambda_- - M)x_\eta = 0 \end{aligned} \tag{19}$$

where, using the conventional form $[PQ] \equiv P_1Q_2 - P_2Q_1$

$$\begin{aligned} &a = [AC],\ b = [AD] + [BC],\ c = [BD] \\ &T = [AB],\ S = [BC],\ L = [AE],\ M = [BE] \end{aligned}$$

$\lambda_\pm$, which denote directions of tangent to ξ- and η components of characteristics in xy-plane, are the root of equation:

$$a\lambda^2 - b\lambda + c = 0 \tag{20}$$

and given by

$$\left.\begin{matrix}\lambda_+ \\ \lambda_-\end{matrix}\right\} = \frac{b \pm \sqrt{b^2 - 4ac}}{2a}. \tag{21}$$

Putting $1-(u^2/a^2) = H$, $-uv/a^2 = K$, and $1-(v^2/a^2) = N$, the concerning fundamental equations (15) and (16) are expressed in the following forms:

$$\begin{aligned} Hu_x + Ku_y + Kv_x + Nv_y + \varepsilon(v/y) &= 0 \\ -u_y + v_x &= 0 \end{aligned} \tag{22}$$

Since coefficients for the characteristics are given by

$$a = H,\ b = 2K,\ c = N,\ T = -H,\ S = 2K,\ L = 0, \text{ and } M = \varepsilon(v/y),$$

ξ- and η components of characteristics are, respectively, calculated by

$$\begin{aligned} dy = \lambda_+ dx;\ du + \lambda_- dv + \varepsilon(v/Hy)dx = 0 \\ dy = \lambda_- dx;\ du + \lambda_+ dv + \varepsilon(v/Hy)dx = 0. \end{aligned} \tag{23}$$

From the root of equation: $H\lambda^2 - 2K\lambda + N = 0$, λ_+ and λ_- are given by

$$\lambda_\pm = (K \pm \sqrt{K^2 - HN})/H. \tag{24}$$

Denoting the speed by V and inclination angle of velocity vector by θ, relations $u/V = \cos\theta$, $v/V = \sin\theta$ and local Mach number $V/a = 1/\sin\mu$ reduce the following expressiosn:

$$\begin{aligned} H &= 1 - \left(\frac{u}{V}\right)^2\left(\frac{V}{a}\right)^2 = 1 - \frac{\cos^2\theta}{\sin^2\mu}, \quad N = 1 - \left(\frac{v}{V}\right)^2\left(\frac{V}{a}\right)^2 = 1 - \frac{\sin^2\theta}{\sin^2\mu} \\ K &= -\frac{u}{V}\frac{v}{V}\left(\frac{V}{a}\right)^2 = -\frac{\sin\theta\cos\theta}{\sin^2\mu} \\ \lambda_\pm &= \frac{K}{H} \pm \frac{\sqrt{K^2 - HN}}{H} = \frac{\sin\theta\cos\theta \mp \sin\mu\cos\mu}{\cos^2\theta - \sin^2\mu} = \tan(\theta \mp \mu). \end{aligned} \tag{25}$$

Characteristics equations (23) can be deformed in the following forms. ξ- and η branch are, respectively,

$$\begin{aligned} dy = \tan(\theta - \mu)dx;\ \frac{\cot\mu}{q}dq + d\theta - \varepsilon\frac{\sin\mu\sin\theta}{\cos(\theta-\mu)}\frac{dx}{y} = 0 \\ dy = \tan(\theta + \mu)dx;\ \frac{\cot\mu}{q}dq - d\theta - \varepsilon\frac{\sin\mu\sin\theta}{\cos(\theta+\mu)}\frac{dx}{y} = 0 \end{aligned} \tag{26}$$

where q is the non-dimensional speed V/a_*, which is given by

$$q^2 \equiv \left(\frac{V}{a_*}\right)^2 = \frac{\gamma+1}{\gamma-1}\Big/\left[1 + \frac{2}{\gamma-1}\sin^2\mu\right]. \tag{27}$$

When the state of points A and B in Fig. 5 are known, quantities on the point C, which is given by the intersection of characteristics of ξ branch from B and of η branch from A, can be calculated by the differential equations (26).

For the sake of simplified expressions for the numerical calculations, some quantities are abbreviated as follows:

$$\begin{aligned} E &= \frac{\tan(\theta+\mu)}{2}, \quad F = \frac{\tan(\theta-\mu)}{2}, \quad G = \frac{\cot\mu}{2q} \\ I &= \varepsilon\frac{\sin\mu\sin\theta}{2y\cos(\theta+\mu)}, \quad J = \varepsilon\frac{\sin\mu\sin\theta}{2y\cos(\theta-\mu)}. \end{aligned} \tag{28}$$

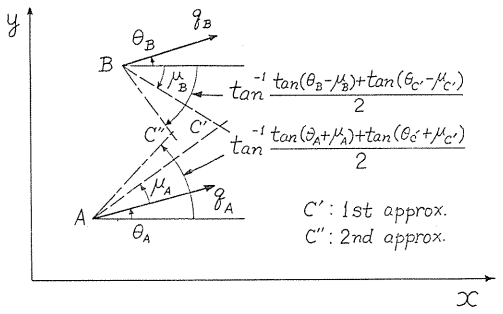

FIG. 5. Elements of characteristics.

Variations along the elements of characteristics are

$$\begin{aligned} y_C - y_A &= (E_A + E_C)(x_C - x_A) \\ y_C - y_B &= (F_B + F_C)(x_C - x_B) \\ (G_A + G_C)(q_C - q_A) - (\theta_C - \theta_A) - (I_A + I_C)(x_C - x_A) &= 0 \\ (G_B + G_C)(q_C - q_B) + (\theta_C - \theta_B) - (J_A + J_C)(x_C - x_B) &= 0. \end{aligned} \tag{29}$$

Quantities on C can be solved formally as follows:

$$\begin{aligned} x_C &= \frac{[y_B - (F_B + F_C)x_B] - [y_A - (E_A + E_C)x_A]}{(E_A + E_C) - (F_B + F_C)} \\ y_C &= \frac{(E_A + E_C)[y_B - (F_B + F_C)x_B] - (F_B + F_C)[y_A - (E_A + E_C)x_A]}{(E_A + E_C) - (F_B + F_C)} \\ q_C &= \frac{(G_A + G_C)q_A + (G_B + G_C)q_B + \theta_B - \theta_A + (I_A + I_C)(x_C - x_A) + (J_B + J_C)(x_C - x_B)}{(G_A + G_C) + (G_B + G_C)} \\ \theta_C &= \frac{\begin{array}{l}[(G_A + G_C)(G_B + G_C)(q_B - q_A) + (G_A + G_C)\theta_B + (G_B + G_C)\theta_A \\ \quad + (G_A + G_C)(J_B + J_C)(x_C - x_B) - (G_B + G_C)(I_A + I_C)(x_C - x_A)]\end{array}}{(G_A + G_C) + (G_B + G_C)} \end{aligned} \tag{30}$$

or

$$\theta_C = \theta_A + (G_A + G_C)(q_C - q_A) - (I_A + I_C)(x_C - x_A).$$

Numerical calculations are started by assuming $E_C = E_A$, $F_C = F_B$, $G_A + G_C = 2G_A$, $G_B + G_C = 2G_B$, $I_C = I_A$ and $J_C = J_B$, and the converged values are obtained by the principle of successive substitution.

In order to take account of the singularity along axis, the mid-point E of characteristic element AC in Fig. 6 (a) is taken, and η branch of characteristic equation (26) is expanded around the point E. Considering $\theta \fallingdotseq 0$ for $\varepsilon = 1$, we have

$$\frac{\cot \mu_E}{q_E}(dq)_E - (d\theta)_E - \frac{\sin \mu_E}{\cos(\theta_E + \mu_E)}\frac{(dx)_E}{y_E}\theta_E = 0 \tag{31}$$

where $y_E/(dx)_E = y_E/\Delta x_{CA} = (1/2)\tan(\theta_E + \mu_E)$ and $\theta_E = (1/2)\theta_C$. Eq. (31) can be deformed as

$$\frac{\cot\mu_E}{q_E}(dq)_E-(d\theta)_E-\frac{\sin\mu_E}{\sin(\theta_E+\mu_E)}\theta_C=0. \tag{32}$$

Introducing $S\equiv(1/2)\sin\mu/\sin(\theta+\mu)$, the characteristic difference equation is obtained as follows:

$$(G_A+G_C)(q_C-q_A)-(\theta_C-\theta_A)-(S_A+S_C)\theta_C=0$$

or putting $\theta_A=0$, we have

$$(G_A+G_C)(q_C-q_A)-(1+S_A+S_C)\theta_C=0. \tag{33}$$

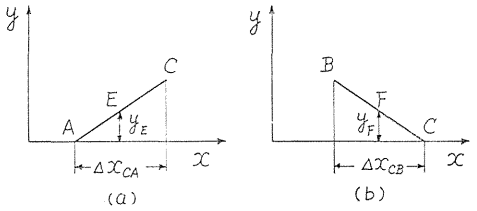

FIG. 6. Characteristic elements at the axis.

In the same way the characteristic equation of ξ branch shown in Fig. 6 (b) is expressed by

$$\frac{\cot\mu_F}{q_F}(dq)_F+(d\theta)_F+\frac{\sin\mu_F}{\sin(\theta_F-\mu_F)}\theta_B=0. \tag{34}$$

Denoting $R\equiv(1/2)\sin\mu/\sin(\theta-\mu)$, the characteristic difference equation is given by using $\theta_C=0$ as follows:

$$\begin{aligned}&(G_B+G_C)(q_C-q_B)+\theta_C-\theta_B+(R_B+R_C)\theta_B=0\\ \therefore\quad&(G_B+G_C)(q_C-q_B)-(1-R_B-R_C)\theta_B=0.\end{aligned} \tag{35}$$

(c) *Calculation of the flow through a conical nozzle of $M=10$*

The nozzle piece of throat section for $M=10$ is shown in the previous Fig. 3. The height of wall boundary from the axis and its inclination are given by

$$h=h_0\left[1+\frac{1}{2!}\left(\frac{h_0''}{h_0}\right)x^2+\cdots\right]=h_0\left[1+\frac{1}{2!}\frac{h_0}{R_0}\left(\frac{x}{h_0}\right)^2+\cdots\right] \tag{36}$$

$$h'=(h_0/R_0)(x/h_0) \tag{37}$$

where the radius of throat is $h_0=6.48$ mm and the radius of curvature of the wall is $R_0=306.52$ mm.

The transonic flow in the throat area is calculated by the above-mentioned method up to $V/a_*=1.002$, whose constant speed line is given by Eq. (28), putting $V/a_*=1.002$. The inclination angle of velocity vector is calculated by the use of Eq. (26) as follows:

$$\theta\fallingdotseq\frac{v/a_*}{V_s/a_*}=h'\frac{y}{h}\fallingdotseq\frac{h_0}{R_0}\frac{x}{h_0}\frac{y}{h_0} \tag{38}$$

In the thin layer along the wall, flows around the corner can by approximately calculated by the theory of two-dimensional Prandtl-Meyer expansion. In the present case it is given.

$$\theta-\theta_*=\sqrt{\frac{\gamma+1}{\gamma-1}}\tan^{-1}\sqrt{\frac{V^2/a_*^2-1}{2/(\gamma-1)-(V^2/a_*^2-1)}}-\tan^{-1}\sqrt{\frac{\gamma+1}{\gamma-1}\frac{V^2/a_*^2-1}{2/(\gamma-1)-(V^2/a_*^2-1)}}. \tag{39}$$

At the corner point, $V/a_*=1.00529$ is calculated by the transonic flow theory and $\theta=0$ in this point. These values determine

$$\theta_*=-0.0004072 \text{ rad}=-1.4'.$$

Five steps of expansion to overall 10 degrees are chosen as shown in the following table.

TABLE 1

V/a_*	1.00529	1.05	1.11	1.17	1.25	1.3235
θ	0°0′	38′	2°3′	3°56′	6°55′	10°0′

Flows in the remaining field are calculated by the method of characteristics described in the preceeding chapter. Lines of characteristics are shown in Fig. 7, 8 and 9. Velocity and Mach number distributions along axis and wall are shown in Fig. 10. Mach number distributions in the test section are shown later in Figs. 16 and 17 comparing with the experimental results.

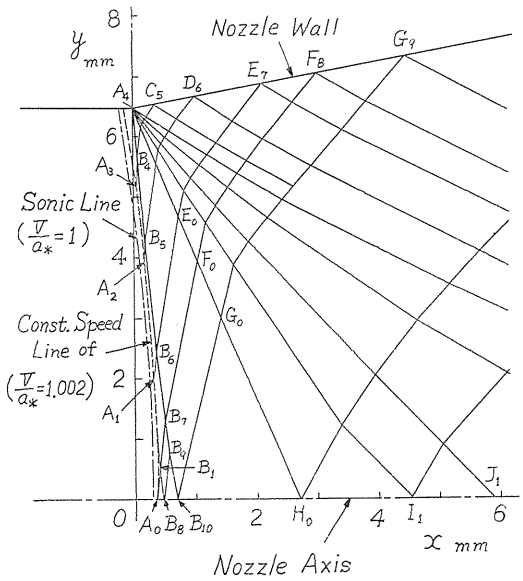

FIG. 7. Characteristic solution at the throat area for $M=10$.

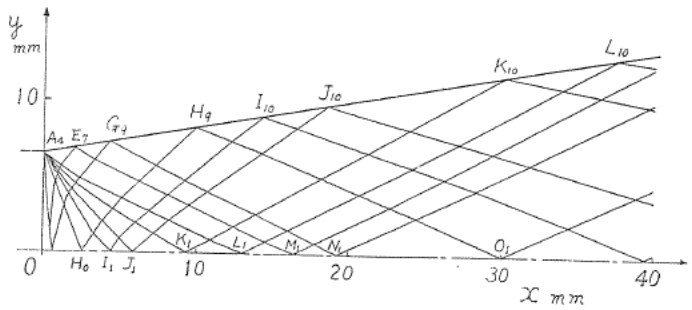

FIG. 8. Characteristics of conical nozzle in the upstream region.

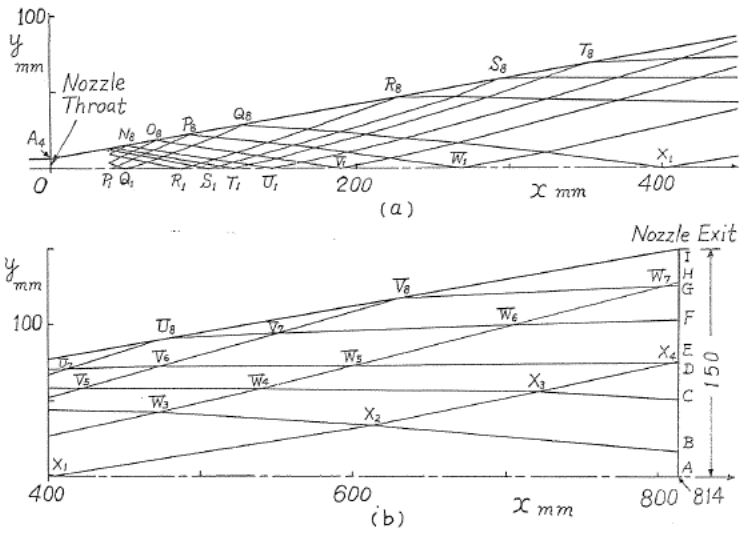

FIG. 9. Characteristics in the main region.

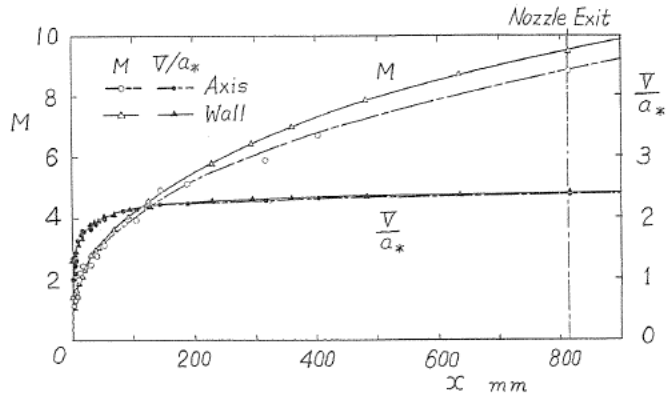

FIG. 10. Calculated velocity distributions.

4. Measurement of the Hypersonic Flow in the Test Section of a Conical Nozzle

In the hypersonic flow through test section, distributions of total pressure behind the shock wave, p_{tb}, are measured by a conical pitot tube with semi-conductor pressure transucer as shown in Fig. 11 (a). To reduce the mechanical impact by the initial shock wave, a plastic foam plate of 1 mm thickness is put on the front surface of diaphragm.

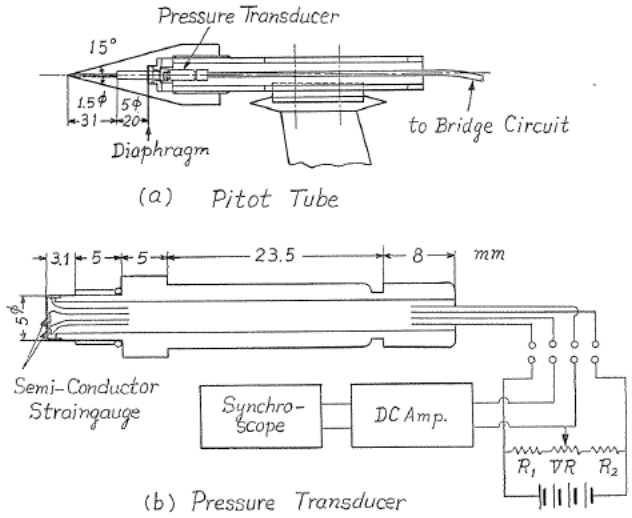

FIG. 11. Pitot tube and semi-conductor pressure transducer.

The principal part of this semi-conductor pressure transducer (Toyoda PMS-5 1 H and 2 H) is a diaphragm attached by two elements of semi-conductor strain gauge, which are arranged to compensate temperature effect. The strong variation of piezo resistance of semi-conductor is measured by the bridge circuit as shown in Fig. 11 (b).

The total pressure at the reservoir condition, p_{ta}, is measured through pressure holes at the end surface of driven tube No. 2 and at the side wall 250 mm upstream from the end as shown in Fig. 12. The pressure trace is detected by Kistler quartz transducers (Kistler 601 H). The piezo electricity is amplified by charge amplifier (Model 504) to record on the synchroscope (Iwasaki DS-5155 and DS-5158 A). Pressure traces of p_{ta} by these two holes show the almost identical pattern as shown in Fig. 13. Since the pressure trace by the hole at the end surface contains some pulsations through the thin duct of 6 mm diameter and of 250 mm length, data by side wall pressure hole are used for the value of p_{ta}.

Experiment in the present report is performed under the following conditions. The driver gas is air of pressure $p_0=40$ kg/cm^2 abs., the driven gas is air of pressure $p_1=1$ kg/cm^2 abs., and the initial pressure of air in dump tank is 10^{-2} mmHg. The piston of weight $W_p=0.400$ kg is used. The gun tunnel is started by breaking the two-stage diaphragm with aluminum plates of 1 mm thickness and its sound of rupture, which is taken by a microphone, is used for the trigger

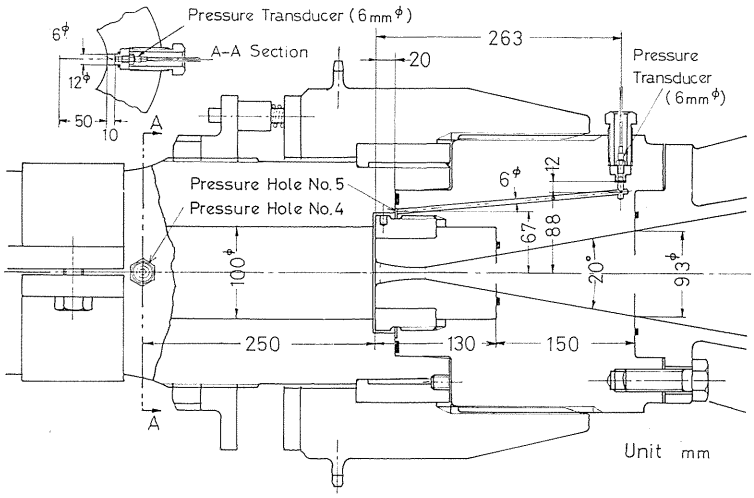

FIG. 12. Reservoir pressure holes and piezo transducers.

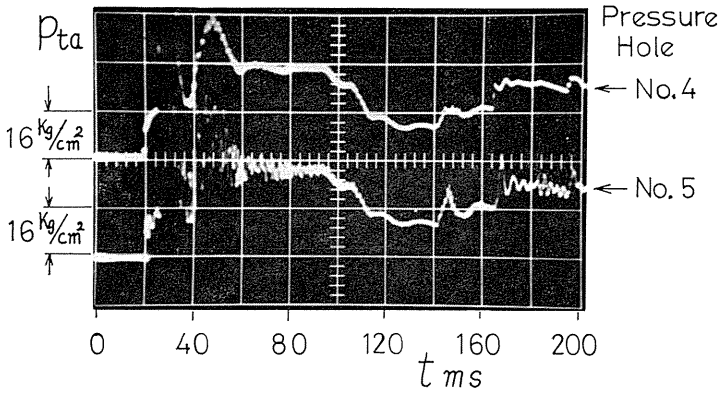

FIG. 13. Reservoir pressure traces.

signal to start the record of synchroscope.

A pressure trace of p_{ta} is shown in Fig. 14 comparing with the schematic $x \sim t$ diagram, where x is taken along the axis of tunnel. Following the burst of diaphragm, compression wave from the piston front grows up to the initial shock wave, which is reflected between the solid surface of nozzle block and the approaching piston surface, and results in the build up of high enthalpy gas at the end of driven tube No. 2. Expansion wave generated at the back surface of the piston moves back to the driving tube and partly reflecting at its entrance section by the discontinuous expansion of sectional area it helps the accerelation of piston. Reflecting expansion wave from the upper end of driving tube No. 1 affect to draw back the piston and makes the state of almost constant reservoir pressure p_{ta}, which can be used as the gas source of hypersonic steady flow through the nozzle. This state is shown as a pressure plateau following the two peaks of pressure trace of p_{ta} in Fig. 14.

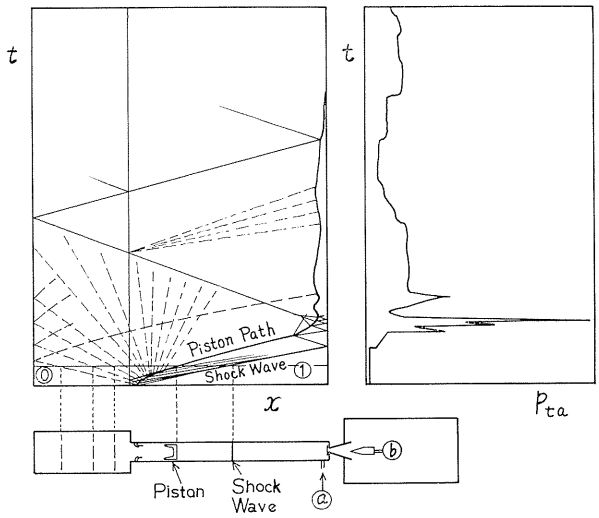

FIG. 14. $x \sim t$ diagram and pitot pressure trace.

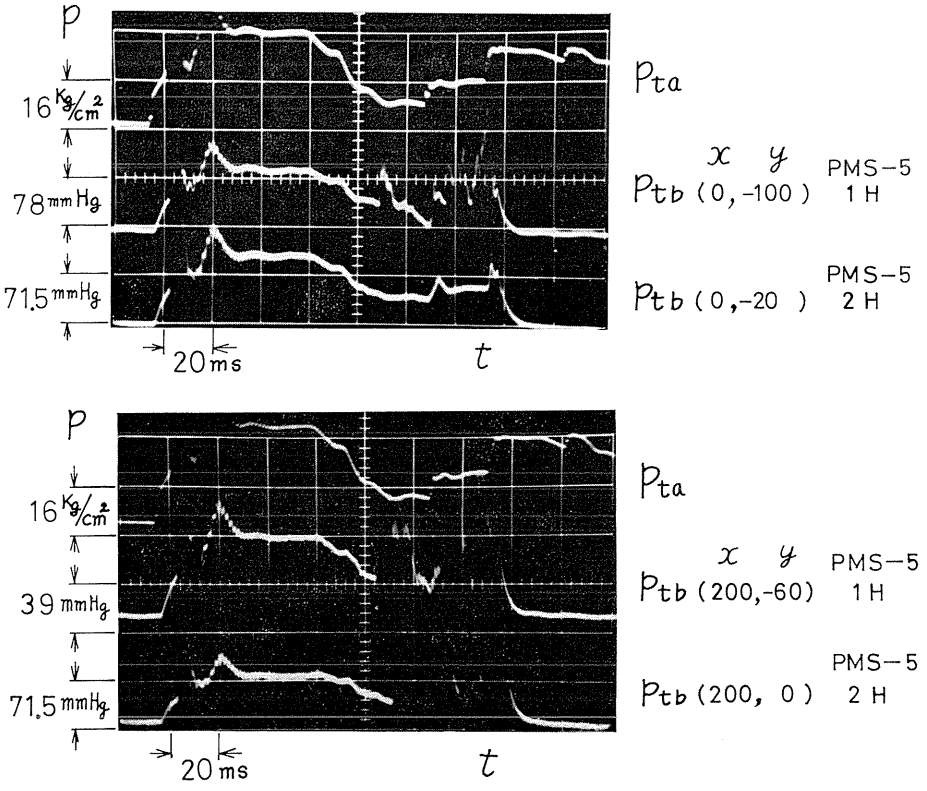

FIG. 15. Pressure traces.

The hypersonic flow through the nozzle is started by the rupture of cellophane membrane, which is sticked at the front surface of the block, with shock wave, and is continued until the exhaust of reserved high energy gas, when the piston is attached to the nozzle block dividing the gases between driven tube and dump tank. In the present work, x and y coordinates are taken along the center line of wind tunnel and horizontally perpendicular to it, respectively, originating at the center of exit section.

Examples of pressure trace of one p_{ta} and two p_{tb} by the dual pitot tubes are shown in Fig. 15. It is found that the steady flow is maintained from $t=50$ ms to 80 ms. In the section of nozzle exit $x=0$ mm, the pressure trace of p_{tb} at $y=-20$ mm shows a good correspondence to that of p_{ta} up to $t=130$ ms. The pressure trace of p_{tb} at $y=-100$ mm shows several peakes of pressure resulting from the pressure variation of p_{ta} after the steady state of flow. This phenomena is observed also in the pressure trace of p_{tb} at $y=0$ mm and at $y=-100$ mm in the section of $x=200$ mm. It may by some effects of vortex generated by non-steady separation of flow from the nozzle wall.

When the total pressures in front of and behind the shock wave of pitot tube are measured, Mach number M of flow can be easily calculated by

$$\frac{p_{tb}}{p_{ta}}=\left[\frac{\gamma+1}{2}M^2\Big/\left(1+\frac{\gamma-1}{2}M^2\right)\right]^{\gamma/\gamma-1}\Big/\left[\frac{2\gamma}{\gamma+1}M^2-\frac{\gamma-1}{\gamma+1}\right]^{1/\gamma-1}. \tag{40}$$

Distributions of measured pressure ratio p_{tb}/p_{ta} and Mach number M along the axis of nozzle are shown in Fig. 16, which is found to give a little higher velocity comparing to the value of calculation. In the conical nozzle the flow is used to be accerelated behind the exit section. Distributions of p_{tb}/p_{ta} and of M along y axis at four sections are shown in Fig. 17. Comparing to the calculation, the measured data show more uniform velocity distributions in the core region, while it is diminished at the outer edge by the effect of boundary- and mixing layer. In the vicinity of exit section, the mean value of velocity is found to be in good agreement with the calculated value.

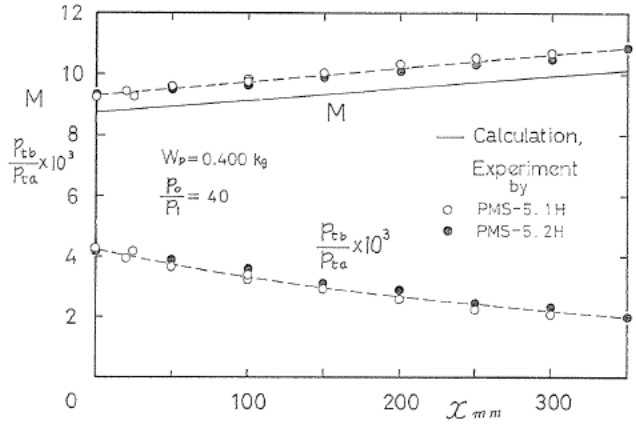

FIG. 16. Distributions of pressure ratio and Mach number along axis.

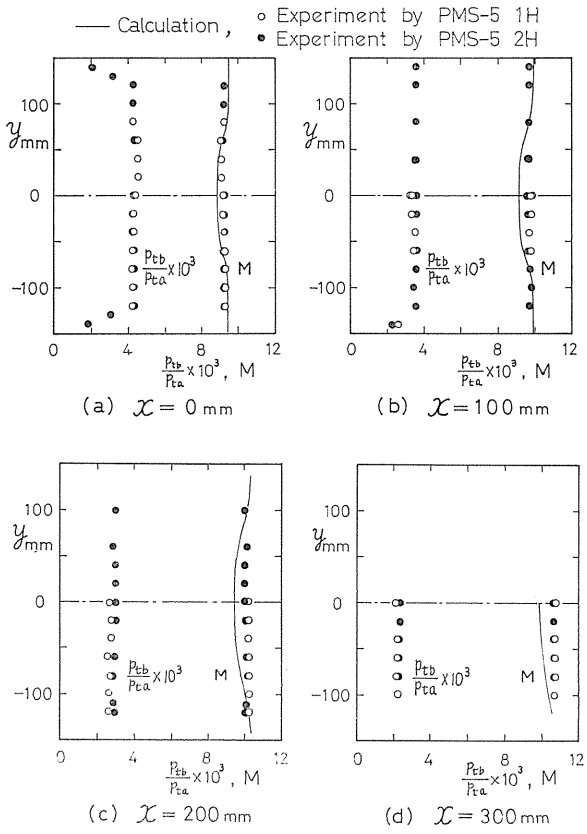

FIG. 17. Sectional distributions of pressure ratio and Mach number.

5. Conclusion

Distributions of total pressure ratio and Mach number at the test section of a conical nozzle in the shock-gun tunnel are measured. Distributions are found to be fairly uniform for the purpose of hypersonic wind tunnel. A practical method of calculation is also reported and the results are compared with to-gether.

References

1) Hall, I. M. and Sutton, E. P., Transonic flow in ducts and nozzles, Symposium Transsonicum, (ed. Oswatitsch, K.), Springer, Berlin, pp. 325-344, 1964.
2) Oswatitsch, K. and Rothstein, W., Das Strömungsfeld in einer Laval-Düse, Jb. dtsch. Lufo Vol. 1, p. 91-102, 1942, transl. as NACA TM 1215; Oswatitsch, K., Gas Dynamics, pp. 474-480, Academic, New York, 1956.
3) Ferri, A., The Method of Characteristics, General Theory of High Speed Aerodynamics, (ed. Sears, W. R.), Princeton Univ., Princeton, pp. 583-669, 1954.